Computers in Biology and Medicine 110 (2019) 175–185

Contents lists available at ScienceDirect

Computers in Biology and Medicine

journal homepage: www.elsevier.com/locate/compbiomed

Dibenzepinones, dibenzoxepines and benzosuberones based p38α MAP kinase inhibitors: Their pharmacophore modelling, 3D-QSAR and docking studies

Mohemmed Faraz Khan[a], Garima Verma[a], Perwez Alam[b], Mymoona Akhter[a], Md Afroz Bakht[c], Syed Misbahul Hasan[d], Mohammad Shaquiquzzaman[a], Mohammad Mumtaz Alam[a,*]

[a] Drug Design and Medicinal Chemistry Lab, Department of Pharmaceutical Chemistry, School of Pharmaceutical Education and Research, Jamia Hamdard, New Delhi, 110062, India
[b] Department of Pharmacognosy, College of Pharmacy, King Saud University, Riyadh, Saudi Arabia
[c] Department of Chemistry, College of Science and Humanities, Prince Sattam Bin Abdulaziz University, P.O. Box- 173, Al-Kharj, Saudi Arabia
[d] Department of Pharmaceutical Chemistry, Faculty of Pharmacy, Integral University, Lucknow, 226026, India

ARTICLE INFO

Keywords:
3D-QSAR
Pharmacophore modelling
Molecular docking
p38α MAP kinase inhibitors
Dibenzepinones
Dibenzoxepines
Benzosuberones

ABSTRACT

In the present study, a series of dibenzepinones, dibenzoxepines, and benzosuberones targeting p38α MAP kinase were subjected to pharmacophore modelling, 3D-QSAR and molecular docking studies. The IC_{50} values for these 67 compounds ranged between 0.003 and 6.80 μM. A five-point model (DDHHR.8) was generated using these compounds. This model was found to be statistically significant and was found to have high correlation (R^2 = 0.98), cross-validation coefficient (Q^2 = 0.95) and F (330) values at six component PLS factor. Tests were performed to ascertain the efficacy of the generated model. These tests included external validation, Tropsha's test for predictive ability, Y-randomisation test and domain of applicability (APD). In order to check the restrictivity of the model, enrichment studies were performed with inactive compounds by using decoy set molecules. To evaluate the effectiveness of the docking protocol, the co-crystallised ligand was extracted from the ligand-binding domain of the protein and was re-docked into the same position. Both the conformers were then superimposed, suggesting satisfactory docking parameters with an RMSD value of less than 1.0 Å (0.853 Å). A 10 ns molecular dynamics simulation confirmed the docking results of the 3UVP-ligand complex and the presumed active conformation. The outcome of the present study provides insight into the molecular features that promote bioactivity and can be exploited for the prediction of novel potent p38α MAP kinase inhibitors before carrying out their synthesis and anticancer evaluation.

1. Introduction

Owing to more than one hundred types of tumors, tackling cancer has become a great challenge [1]. Cancer is characterised by the proliferation of abnormal cells and is one of the foremost causes of death across the globe. Surgery, chemotherapy and radiotherapy are the standard strategies employed in the treatment of this disease [2]. An escalating trend has been reported in the number of cancer patients, particularly in developed nations. In spite of the tremendous progress made in cancer treatment, there is a pressing need for the development of novel and effective anticancer agents. The non-selective nature of current therapeutics, along with the associated side effects, continues to be the major driving force for drug development [3].

Different tyrosine kinases and cytokine receptors in conjunction with heterotrimeric G proteins are primarily responsible for the activation of intracellular protein such as serine/threonine kinases, referred to as mitogen-activated protein kinases (MAPKs) [4]. They are known to regulate different cell functions like cell progression, proliferation and inflammatory responses to stress signals [5]. Extracellular signal-regulated kinases 1/2 (ERK1/2), c-Jun N-terminal kinases (JNK), p38 and ERK5 proteins are the four major members of MAP kinase family. Activation of MAP kinases is associated with the commencement and advancement of several cancers and inflammatory disorders. Due to their significant roles in cell differentiation and proliferation, medicinal chemists see these kinases as fascinating and exploitable targets for the development of anticancer agents.

MAPKs are known to act as molecular switches and demonstrate at least two conformations, which represent the catalytically active and

* Corresponding author. Department of Pharmaceutical Chemistry School of Pharmaceutical Education and Research, Jamia Hamdard, New Delhi, 110062, India.
E-mail addresses: drmmalam@gmail.com, mmalam@jamiahamdard.ac.in (M.M. Alam).

https://doi.org/10.1016/j.compbiomed.2019.05.023
Received 3 December 2018; Received in revised form 30 May 2019; Accepted 30 May 2019

Table 1
Score of different parameters of the hypotheses.

S. No.	Hypothesis	Survival Score	Survival Inactive	Site	Vector	Matches	Activity	Inactive
1.	DDHRR.8	6.103	4.382	0.72	0.873	7	8.000	1.720
2.	DDHRR.9	6.090	4.319	0.72	0.877	7	8.000	1.771
3.	DDHRR.24	5.961	4.340	0.69	0.842	7	8.301	1.621
4.	DDHRR.22	6.071	4.295	0.68	0.890	7	8.301	1.776
5.	DDHRR.7	5.940	4.245	0.62	0.845	7	8.000	1.695
6.	DDHRR.23	5.694	3.961	0.58	0.857	7	8.301	1.733
7.	ADHRR.53	5.893	4.207	0.63	0.965	7	8.000	1.686
8.	ADHRR.52	5.858	4.173	0.62	0.965	7	8.000	1.685
9.	ADHRR.54	5.896	4.287	0.63	0.931	7	8.000	1.609

D: Donor; A: Acceptor; H: Hydrophobic; R: Aromatic ring.

inactive states of the enzyme. One of the necessities for MAPKs to be in the active form is post-translational phosphorylation of key residues present at the activation loop [6]. These kinases are activated by phosphorylation on Thr and Tyr within a Thr-X-Tyr motif by a specific upstream MAP kinase, where X is Pro, Glu and Gly for ERK, JNK and p38, respectively. Since the Thr-X-Tyr motif is located on the surface loop close to the active site, the loop is often termed the 'phosphorylation lip' or 'activation lip.' Inactivation is brought about by the action of phosphatases on the same motif [7].

Currently, ligand- and structure-based approaches as well as OR, along with computational studies, are used as constructive tools for the development of novel medicinal agents. Since the 1970s, there has been tremendous growth in quantitative structure-activity relationship (QSAR) studies in the field of medicinal chemistry. A mathematical relationship linking chemical structure and pharmacological activity or another property for a series of compounds in a quantitative manner is the aim of QSAR [8,9]. Our group has already reported two such computational studies recently [10,11]. Computational work on MAP kinases are of great interest to researchers [12–14].

2. Materials and methods

2.1. Data set

The present *in silico* study utilised a set of 67 compounds containing dibenzepinones, dibenzoxepines and benzosuberones from the available literature [15]. Compounds chosen for inclusion into the data were assayed utilising a similar method [16]. The structures and potency profiles of the compounds were found to have significant variations. The data set was comprised of compounds having IC_{50} values ranging from 0.003 to 6.80 μM (pIC_{50}: 8.523 to 5.167). These IC_{50} values were converted into molar values. Utilising the following formula, these values were further converted into pIC_{50} values.

$$pIC_{50} = -\log_{10} [IC_{50}]$$

The builder panel in Maestro was used for generating the 3D structures of ligands. Subsequently, optimisation was performed using the Lig Prep module present in Schrödinger 2016–1, v3.1. Partial atomic charges were attributed followed by the generation of ionisation states around a pH of 7.0. Low energy conformers were generated using the OPLS_2005 force field [17]. For every individual ligand, energy minimisation was optimised until it achieved a root mean square deviation (RMSD) cut-off of 0.01 Å. Finally, the resulting molecules were available for modelling studies.

2.2. Pharmacophore 3D-QSAR modelling

For generating 3D-QSAR and the pharmacophore model for p38α MAP kinase inhibitors, Phase (v4.6, Schrödinger 2016–1) was selected [18,19].

The ligands thus prepared were taken for developing the pharmacophore model panel of Phase with the corresponding biological activity data. These ligands were allocated as active or inactive by keeping a threshold pIC_{50} in the range of 7.99 to 5.40. The remaining molecules were considered to be moderately active. For flexible ligand superposition, Phase (v4.0) has been recognised to be an important tool [20,21]. Hence, flexible alignment of the selected p38α MAP kinase inhibitors was done using Phase (v4.0) shape screening. Compound **48**, the most potent molecule, was taken as the template, while the default setting was applied with pharmacophore type volume scoring. As per the default settings, up to 100 conformers and a maximum of 10 conformations for each rotatable bond were generated. These conformations were varied and thus at most one alignment was retained for each ligand. Random selection was performed, choosing the automated random selection option available in the Phase (v4.0) module for assigning the training and test sets for 67 compounds. Twenty percent of the compounds (13 compounds) were included in the test set whereas the remaining 80% (54 compounds) were incorporated into the training set. Certain default chemical features of Phase were included by pharmacophore sites for these compounds: two hydrogen bond donors (D), a hydrophobe (H) and two aromatic rings (R). Tolerance for pharmacophore matching was assigned at 1 Å. Sixteen variants were produced by taking the maximum and minimum number of sites as 5 and 4, respectively. At least 7 of the actives were matched. In total, 230 possible combinations of features were finally obtained that could generate common pharmacophores. The generated hypotheses were scored and ranked in accordance with their vector, volume, survival scores, survival actives and site scores [18]. Table 1 represents the scores of different parameters of few top resulting hypothesis.

Five sites were found to be common in the generated hypotheses for all selected compounds. Partial least square (PLS) regression statistics were used for generating the 3D-QSAR model by keeping the grid spacing of 1 Å. A progressive increase in the statistical significance and predictivity was adjusted to six PLS factors and hence this value was taken as 6 for model development (Table 2).

Fig. 1a and b represent the distance and angles amongst various sites of the model DDHRR.8, respectively. This is also shown in Table S1 and Table S2 of the **Supplementary Material**. The generated common pharmacophore along with the aligned actives and inactives superimposed over it is represented in Fig. 2a and b. Evaluation of the fitness score of all the ligands was done using the model DDHRR.8 (Table S3; **Supplementary Material**). To identify the requirements of distinct imperative pharmacophore at spatial sites of structure, contour plot analysis was performed.

2.3. Model validation

The best pharmacophoric model characterised was the six-component PLS factor QSAR model DDHRR.8. Model validation was measured in terms of accuracy in the activity estimation of the ligands of the training set. A significant linear correlation was observed in scatterplots for the experimental and predicted activities of ligands. Only a marginal

Table 2
PLS statistical parameters of the model DDHRR.8

PLS	SD	R^2	F	P	Stability	RMSE	Q^2	Pearson-R
1	0.7053	0.4842	48.8	5.201e-009	0.8324	0.5664	0.6243	0.7945
2	0.4561	0.7884	95	6.316e-018	0.6216	0.4161	0.7972	0.8967
3	0.3417	0.8836	126.5	2.4e-023	0.583	0.3156	0.8833	0.9423
4	0.2568	0.9356	177.9	1.594e-028	0.4868	0.2783	0.9093	0.9536
5	0.1957	0.9634	252.3	3.117e-033	0.4243	0.2152	0.9458	0.9727
6	0.1573	0.9768	330	1.144e-036	0.3836	0.215	0.9459	0.9726

SD: Standard deviation of regression, R^2: Regression coefficient; F: Ratio of the model variance to the observed activity variance (variance ratio); P: Significance level of variance ratio; Q^2: Cross validated correlation coefficient for the test set; RMSE: the RMS error in the test set predictions.

difference was found between the experimental and predicted values (Fig. 3a and **3b)**. External validation was also employed in order to ascertain the effectiveness of the model DDHRR.8. Same biological tests were used for compounds of both the 'internal' training and test sets and the 'external' test set. It is necessary to mention here that compounds of the training and test sets share structural similarity, whereas the external test set compounds belong to a separate publication. This is to clearly differentiate between the test and the external test set utilised in the study. Further reliability of the model was established by performing this external validation. For the external training set compounds, graphs of actual *vs.* predicted value and residual *vs.* predicted value were plotted and are shown in Fig. S1 of the **Supplementary Material**. The calculated pIC_{50} values for these compounds are given in Table S4 of the **Supplementary Material**.

Enalos model acceptability criteria KNIME node was utilised to test the predictive power of the generated pharmacophore model [22,23]. This includes all tests reported earlier by Tropsha [24,25]. In generating the predictors of activity/property, particularly in the case of

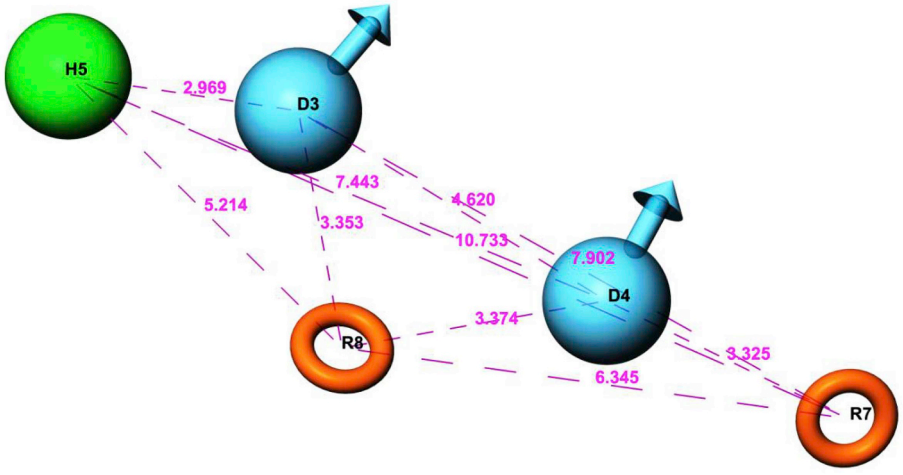

a

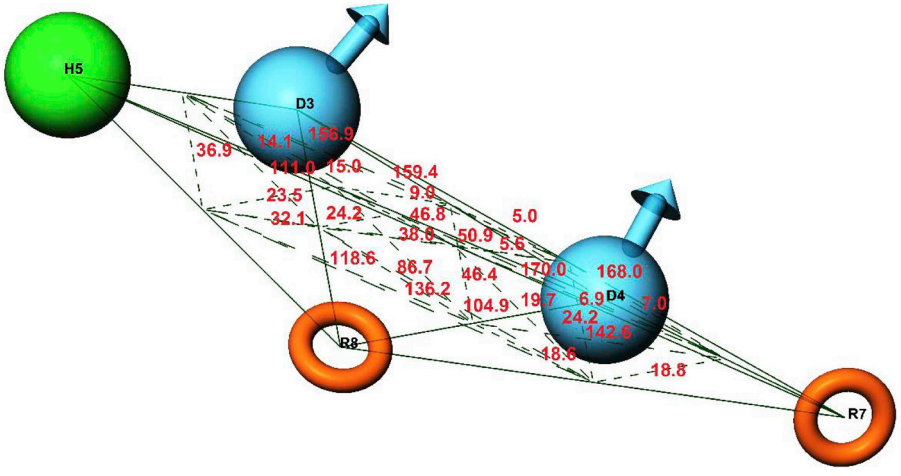

b

Fig. 1. Intersite **(a)** distances and **(b)** angles between the pharmacophoric points of model DDHRR.8. All distances are in Å unit. Sky blue spheres with arrow, hydrogen bond donor (D); orange open circle, aromatic ring (R); green sphere, hydrophobe (H). (For interpretation of the references to colour in this figure legend, the reader is referred to the Web version of this article.)

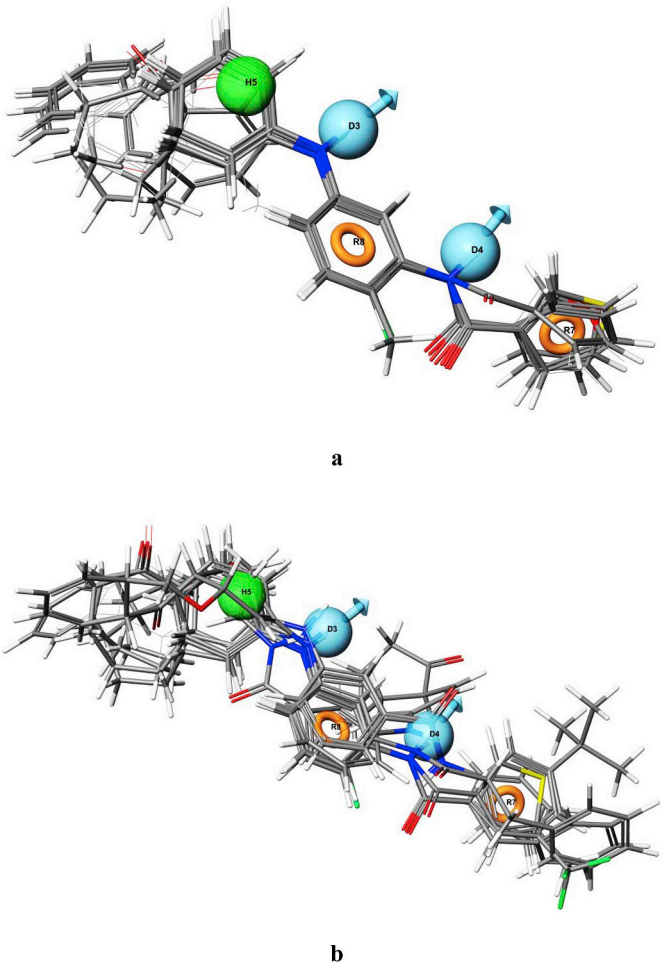

Fig. 2. (a) Mapping of the active compounds onto the pharmacophore. (b) Mapping of inactive compounds onto the pharmacophore.

continuous QSAR, the conditions to be followed are presented as: (i) coefficient of correlation R among the predicted and observed activities; (ii) determination coefficients (predicted versus observed activities R_0^2 and observed versus predicted activities ${R'}_0^2$ for regressions through the origin); (iii) slopes k and k' of the regression lines through

Criterion	Assessment	Result
R^2 > 0.6	PASS	R^2 = 0.945
Rcvext^2 > 0.5	PASS	Rcvext^2 = 0.945
(R^2-R0^2)/R^2 < 0.1	PASS	(R^2-R0^2)/R^2 = 0.004
(R^2-R'0^2)/R^2 < 0.1	PASS	(R^2-R'0^2)/R^2 = 0.0
abs(R0^2-R'0^2) < 0.1	PASS	abs(R0^2-R'0^2) = 0.003
0.85 < k < 1.15	PASS	k = 0.999
0.85 < k' < 1.15	PASS	k' = 1.0

Model Predictive

a

Reliable percentage equals 100.0% (13 out of 13)
Unreliable percentage equals 0.0% (0 out of 13)
The limit is 0.056

b

Fig. 4. Screenshot of results obtained by **(a)** Enalos Model Acceptability Criteria KNIME node for Tropsha's validation; **(b)** Enalos Domain- Leverage node for Applicability Domain.

the origin. The left column of Fig. 4a and Table S5 of the **Supplementary Material** represent the Tropsha parameters and their acceptable ranges, whereas the right column depicts the obtained results.

In order to further validate the developed model, enrichment studies utilising the decoy test were incorporated into the workflow. The generated model's predictive power was evaluated by a generic dataset of 1000 drug-like molecules that constituted the decoy test set compounds [26]. These ligand decoy sets are available for download from the Schrödinger database. The decoy database was generated using the Generate Phase database subapplication window of the Phase application [19,27]. To ensure consistency of the selected model and accurate ranking of the compounds, enrichment factor (EF) and robust initial enhancement (RIE) were studied [28].

Moreover, in order to compute the statistical parameters for external validation, the Xternal Validation Plus 1.2 tool was employed. The aforementioned tool was utilised (i) to evaluate the prediction quality of a QSAR model based on the mean absolute error (MAE) criterion [29] and (ii) to search for the presence of any bias in the prediction errors of the test set compounds [30].

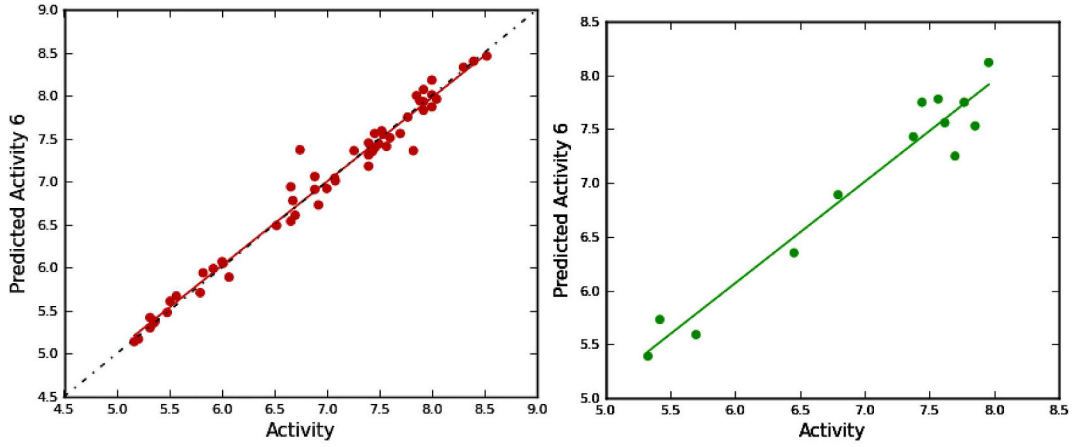

a **b**

Fig. 3. Scatter plot of the observed versus phase-predicted activity for **(a)** training set compounds with best fit line y = 0.98x + 0.16 (R^2 = 0.98) and **(b)** test set compounds with best fit line y = 0.94x + 0.40 (R^2 = 0.95).

2.4. Domain of applicability

The domain of applicability (APD) must be defined in order to screen a QSAR model for any new compounds [25,31]. Compounds falling into such a domain are considered eligible for prediction. One of the simple approaches to determine this parameter is the extent of extrapolation [25]. It depends on a calculation of the leverage (h_i) for every molecule, which utilises the quantitative structure-property relationship (QSPR) model for the prediction of bioactivity.

2.5. Y-randomisation test

The robustness of a QSPR model is ensured using the Y-randomisation technique [25,31]. To generate a new QSPR, the dependent variable vector was randomly shuffled. The procedure was repeated many times. The new QSPR model thus generated anticipated low R^2 and Q^2 values upon shuffling. If the results are contrary to those expected, the obtained QSPR model cannot be accepted [32].

2.6. Molecular docking

The RCSB protein data bank was used to retrieve the catalytic portion of the p38α MAP kinase complex with benzamide substituted benzosuberone (**PDB Id:** 3UVP). Protein preparation was then performed by the protein preparation wizard available in Schrödinger suite 2016–1 [33]. The crystallographic water molecules that were unable to form a minimum of three hydrogen bonds were removed by the wizard. With the addition of hydrogen bonds corresponding to pH 7, appropriate ionisation states for acidic and basic amino acid residues were taken into consideration. Energy minimisation of the crystal structure was performed by the OPLS_2005 force field [17]. The radii (15 Å) around the ligand in the crystal structure was defined as the active site, at a centroid of which the grid box was generated. Conformers with lower energy were docked into the active site of MAP kinase protein (**PDB Code:** 3UVP) *via* grid-based ligand docking with Energetics (Glide v7.0, Schrödinger 2016–1) [34,35] in the absence of any constraint in extra precision mode. Parameters such as glide energy, glide score function and glide E model energy were selected for the identification of the best docked structure. Among the docked compounds, compound **48** was found to have more negative binding energy and was taken for further study. For inhibitor **48,** hydrophilic and hydrophobic field maps were also generated.

2.7. Docking validation protocol

The accuracy of the obtained results was validated by extracting the co-crystallised ligand from the ligand binding domain of the protein and re-docking it into the same position. The lowest energy pose obtained after re-docking and the co-crystallised ligand obtained through X-ray crystallography in the protein used in the study were superimposed. Finally, the RMSD between the predicted conformation and the observed X-ray crystallographic conformation was determined [19,35,36].

2.8. Binding free energy calculation using the Prime/MM-GBSA approach

In order to minimise the energy of the docked poses, a local optimisation feature in Prime (Schrödinger 2016–1, v3.1) [37] was utilised and the molecular mechanics-generalised born surface area (MM-GBSA) continuum solvent model was used for computing the binding free energies of the complex (Table S11**, Supplementary Material**). The method includes the VSGB solvent model [38], the OPLS_2005 force field [17] and rotamer search algorithms.

2.9. Molecular dynamic simulations

Molecular dynamic (MD) simulations were carried out for the docked complex with compound **48** using Desmond version 4.4 (Schrödinger suite). This protocol was followed for the drug-target complexes, i.e. the compound **48**-MAP kinase complex. The protein was set in water for solvation using the TIP3P box. Following solvation, charge neutralisation was carried out by the addition of Na^+ and Cl^- ions. Minimisation was carried out for the total box that contained protein, water and ions for 2000 steps using the steepest descent algorithm and then for 3000 steps using a conjugate gradient. The structure was analysed for its stability and potential energy after the completion of these steps. The total system was then equilibrated. MD for 10 ns was run for the final equilibrated structure. The simulation was performed under conditions of constant temperature and pressure. The Martyna-Tobias-Klein scheme was used for pressure coupling. All runs were performed at 300 K at a constant volume and temperature with the NPT ensemble. The trajectory file was further analysed for RMSD, root mean square fluctuation (RMSF), hydrogen-mediated bonding interactions and van der Waals interactions.

3. Results

3.1. Pharmacophore and 3D-QSAR models

Development of the pharmacophore model was done in Schrödinger 2016–1, Phase (v4.0) module [18]. The effect of substituents on activity was mainly revealed by atom-based 3D-QSAR. To develop a hypothesis, maximum of five features were accepted depending on the site. Furthermore, several common hypotheses were developed for all 67 compounds. The results of the top eight hypotheses are tabulated in Table 1. The best fitted model DDHRR.8 (R^2 = 0.9768, Q^2 = 0.9459 and F = 330) featured two aromatic rings, two hydrogen bond donors, one hydrophobic centre (Fig. 1a and b) and had a maximum survival score of 6.103. The comparison made by deducing survival inactive from survival active also made this evident. The inactive features were removed from the hypothesis and were conclusively maximum for the DDHRR.8. Intersite distances and angles between site points were established as the major attributes amongst the pharmacophore features. The alignment of pharmacophore hypothesis DDHRR.8 overactive ($pIC_{50} > 7.99$) (Fig. 2a) and inactive ($pIC_{50} < 5.40$) (Fig. 2b) compounds confirmed the interstitial site distances to be the major point of difference between the active and inactive compounds.

3.2. Model validation

Based on the active compounds, a cross-validation coefficient (Q^2 = 0.9459) (Table 2) was determined to predict and validate the common pharmacophore model, DDHRR.8 (test set). The regression coefficient (R^2) of the training set was found to be 0.9768, exhibiting the relevance of the model. On a maximum scale of 1, the generated model showed a stability value of 0.8324 and an F value of 330. Moreover, a high degree of confidence on the model was attributed by the P value of 1.144e-036 and Pearson's R of 0.9726. For the estimation of unknown compounds in the test set, the generated model's stability was indicated by the standard deviation (SD) value of 0.1573 and the RMSE of 0.215.

To evaluate the efficacy of the generated model, further validation was done using an external test set [39]. Table S3 **(Supplementary Material)** represents the calculated pIC_{50} values of the compounds included in the predicted set. Table S4 **(Supplementary Material)** displays the predicted values for the external test set. Fig. S1a **(Supplementary Material)** shows the plot of experimental *vs.* predicted pIC_{50} values of the external test set and the plot of residual *vs.* predicted

values is presented in Fig. S1b **(Supplementary Material)**. To determine the predictive ability of QSAR, these two models are very important. To identify outliers from the QSAR model, scatter residual plots were made [40]. No outlier was found in the study (supported by Fig. S1b **(Supplementary Material)**. Comparison of the number of compounds taken in the test and number of dots present in the scatterplot help in determining the presence or absence of outliers in the study. Since in this case both the numbers were the same, the model was stable and reliable. This also supports the experimental pIC_{50} values for the compounds available in the external test set. For the external test set, a predictive correlation coefficient R^2 value of 0.90 was observed. A QSAR model is considered good when the R^2 value is more than 0.5 among the predicted and experimental values and reflects its ability to predict the inhibitory activity of compounds that were not included in the development of the model [40,41].

Additionally, the Enalos model acceptability criteria KNIME node was also used in the data. Tropsha's recommended tests [27] for determining the predictive ability of a model exhibited positive results and are presented in Fig. 4a. The results suggest that such alignment can be efficiently taken into consideration in the ligand-receptor interactions. Therefore, the generated QSAR model is considered reliable and can be utilised for designing new p38 MAP kinase inhibitors within this structural motif of compounds.

Furthermore, the model was screened against 1000 decoy molecules based on the Schrödinger database to validate its discriminatory ability. This model had ability to find all the active compounds present in a hit list. In order to determine the significant contribution of active compound ranking in the enrichment, robust initial enhancement (RIE) was calculated for the generated model. The RIE value for DDHRR.8 was found to be 10.84, which is a clear indication of the superiority of the pharmacophore model ranking over random distribution.

In order to test the performance of the generated model, another factor that is considered reliable is AUC of the ROC curve. DDHRR.8 exhibited a significant AUC value of 0.97 and ROC of 0.99 (Fig. S2 & Tables S6–S9 of **Supplementary Material**).

On the basis of results obtained by MAE-based criteria, the prediction quality of the model was found to be good. After removing 5% of test set objects with high residual values, the MAE and MAE + 3*SD values of the model were found to be 0.1513 and 0.481, respectively. The model also passed the model biasness test. The systematic error or bias in model predictions were found to be absent on analysing the prediction errors of the test set compounds. The results of the statistical parameters for external validation are summarised in Table S10 of the **Supplementary Material**.

3.3. Domain of applicability

To check the reliability of model validation, we assessed the APD of our model. In order to define the APD of the generated model, the Enalos domain leverage (extent of extrapolation) node was included in our procedure. Based on the equation provided in the Methods section, the APD limit was defined as 0.231 in this method. As a result of the APD assessment, none of the compounds were found to be outliers as all the compounds fell within the range (Fig. 4b). Thus, all the compounds were considered to be reliable as none of the compounds were outside the domain of the applicability.

3.4. Y-randomisation test

The model was further validated using the Y-randomisation test. Ten shuffles of the Y vector were made randomly. Values of R^2 and Q^2 were found to be low. This revealed that the results obtained from the original model were not because of structural dependency or chance correlation in the training set. The R^2 values were found to be in the

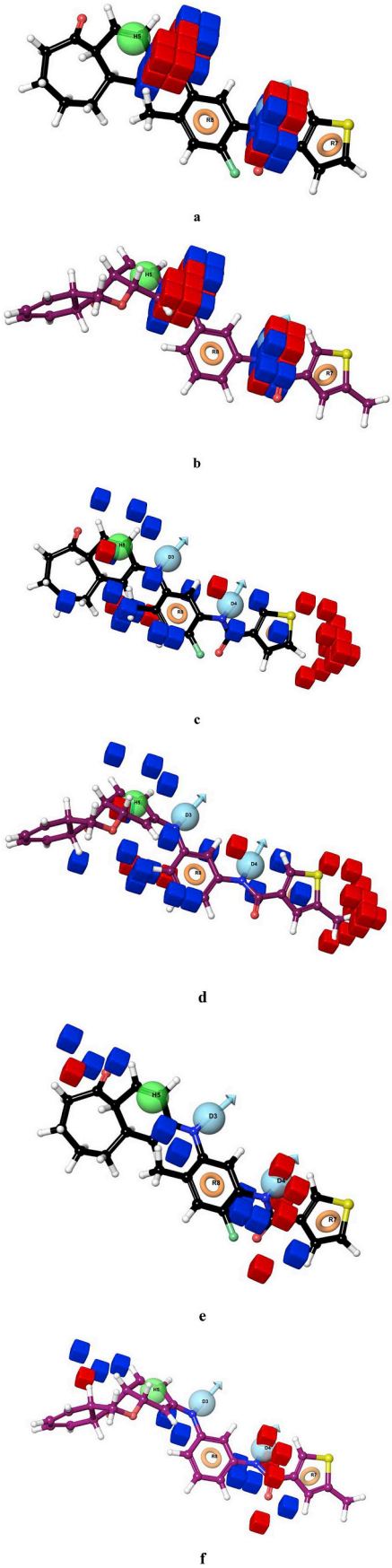

a

b

c

d

e

f

(caption on next page)

Fig. 5. QSAR model visualized in the context of favorable and unfavorable hydrogen bond donor effects in **(a)** compound **48** (8.523) and **(b)** compound **66** (5.167). QSAR model visualized in the context of favorable and unfavorable hydrophobic interactions in **(c)** compound **48** (8.523) and **(d)** compound **66** (5.167). QSAR model visualized in the context of favorable and unfavorable electron withdrawing groups in **(e)** compound **48** (8.523) and **(f)** compound **66** (5.167).

range of 0.04–0.375 and the Q^2 values were found to be between 0.00 and 0.12.

3.5. 3D-QSAR contour map analysis

The effect of spatial arrangement of some structural features like H-bond donors and H-bond acceptors, as well as electrostatic, hydrophobic and ionic interactions on MAP kinase inhibitory activity was evaluated by contour plot analysis in the 3D-QSAR study. The positive and negative contribution of an individual feature is indicated by blue and red cubes, respectively. Some of the most favorable and unfavorable interactions found through the QSAR model for the most active and least active ligands are presented in Fig. 5a–f. The results of our study and those reported by the researchers who have synthesised and biologically evaluated these compounds were found to be in concordance [15].

Several important components that impact the MAP kinase inhibitory activity, including the hydrogen-bond donor nature (Fig. 5a and b), hydrophobic character (Fig. 5c and d) and electron withdrawing group (Fig. 5e and f) were compared for the most active compound **48** (Fig. 5a, c, 5e) and the least active compound **66** (Fig. 5b, d, 5f). In all the figures, regions favouring the aforementioned effects are indicated by blue cubes and the regions that are unfavorable for the same are represented by red cubes.

3.6. Molecular docking and binding free energy calculations using the Prime/MM-GBSA approach

Molecular docking scores and free binding energies MM-GBSA [38], a related post-scoring approach, for the MAP kinase (PDB ID: 3UVP) enzyme were evaluated and are given in Table S11 **(Supplementary Material)**. Amongst 67 listed total scores, most of the compounds were found to have a glide score in accordance with the pIC_{50} values. This was confirmed by the docking study showing that the interactions were mainly dominated by hydrophobic and aromatic functionality because of the presence of a phenyl ring and a thiophene moiety. Due to pronounced presence of the active site in the region of the Lys 53, Glu 71, Phe 169 and Asp 168 amino acid residues, most of the interactions were found in that region (Fig. 6a and b). Amino acid residues Val 105, Ala 51, Val 52, Leu 104, Leu 86, Ile 146, Leu 74, Leu 75, Met 78, Phe 169, Ile 84, Leu 167, Leu 108, Val 30 and Val 38 were found to be responsible for hydrophobic interactions (Fig. 6c). This can be very easily observed by the map analysis, generated by hydrophobic and hydrophilic fields for inhibitor **48** (Fig. 7a), where the phenyl and thiophene moieties are completely buried in the hydrophobic pocket (shown in orange) while the atoms of the amide (oxygen and nitrogen), ketone (oxygen) and halogen (fluorine) groups are present in the hydrophilic pocket (shown in cyan). This was found to be in agreement with the 3D-QSAR results where the hydrophobic R7 (thiophene moiety) and R8 (phenyl ring) pharmacophoric features of **48** were found to have a positive impact on activity (Fig. 6c). The sulphur atom of the thiophene moiety was found to play a vital role in the stabilisation of the inhibitor at the active site, as indicated by the results obtained by our Glide XP-docking. Solvent exposure in the region of the suberone ring and Ser 32, Ser 37, His 107, Thr 106, Asn 155 and Ser 154 were responsible for polar interactions of the molecule with the receptor. The compound was also found to establish a hydrogen bond with the backbone of amino acid Asp 168 and the side chain of Glu 71. A π-π interaction between the thiophene ring and Phe 169 was also seen. Additionally, a salt bridge between the phenyl ring and Lys 53 was also formed (Fig. 6a and b).

Fig. S3 of the **Supplementary Material** displays the binding pattern and 2D ligand interaction diagram of the least active compound of series (**66**). The compound was found to have polar interactions with amino acid residue Thr 106. Hydrophobic interactions with the compound were found with amino acid residues Val 30, Val 38, Leu 104, Phe 169, Leu 74, Leu 75, Leu 167, Ile 84 and Ala 51. Asp 168 and Glu 71 were the residues responsible for negatively charged interactions. Overall, the extent of interactions for the most active compound (**48**) was much greater as compared to that exhibited by the least active compound (**66**).

To estimate the free energy of binding for the best-docked complexes from Docking, Prime/molecular mechanics generalised born surface area (Prime/MM-GBSA) calculations were applied. The MM-GBSA calculations inferred compound **48** with a binding free energy of −89 kcal/mol, found to have the most profound inhibitory nature among all the compounds interacting with MAP kinase.

3.7. Docking validation protocol

Furthermore, the docking procedure's accuracy was ascertained by investigating the closeness of the minimum energy poses (binding conformation) which was produced by object scoring functions and the glide score (G score), which bear a resemblance to the one determined through X-ray crystallography. A root mean square deviation (RMSD) of 0.356 Å was found between the predicted and the observed X-ray crystallographic conformation of the co-crystallised ligand (benzamide substituted benzosuberone) (**PDB Code:** 3UVP) (Fig. 6d). The RMSD value thus obtained experimentally is suggestive of the reliability of glide XP docking mode in reproducing the observed binding pattern of MAP kinase inhibitors. Moreover, the superposition of the best XP docking pose conformation of **25** and 3D-QSAR pose exhibited a similar orientation with an RMSD value of 0.090 Å (Fig. 7b).

3.8. Molecular dynamics simulation

Upon the procurement of trajectories, the structural deviations of the complexes in terms of RMSD, RMSF and other parameters were investigated during the course of 10 ns simulation trajectories. Stability of the protein-ligand complex was also gauged during the 10 ns simulation trajectories. The RMSD of the protein Cα-backbone from its starting position increased to 2.1 Å for the first 3 ns of the trajectory and then became stable around 1.5 Å in the last 7 ns of the simulation. Deviations converged after a simulation time of 3 ns, indicating 0.7 Å of deviation, thus imparting stability to compound, as shown in Fig. 8.

As evident from the histograms and plots shown in Fig. 9, residues like Glu 71, Met 109, Gly 110 and Asp 168 play important roles in p38 MAPK regulation. The interaction fractions of the mentioned amino acid residues were 0.6, 0.9 and 1.0, respectively. Residues like Glu 71, Met 109, Gly 110 and Asp 168 showed hydrogen bonding interactions, while Val 30, Val 38, Ala 51, Lys 53, Leu 74, Leu 75, Ile 84, Leu 108, Ala 157, Leu 167, Leu 167 and Phe 169 showed hydrophobic intercations at the active site pocket of MAP kinase.

As depicted in Fig. 10, the RMSD of the ligand in the binding pocket of MAPK fluctuated between 0.4 and 1.2 Å, inferring its stability with p38 MAPK. In the context of other ligand properties, the solvent accessible surface area (SASA) of the solvent molecule (water) was found

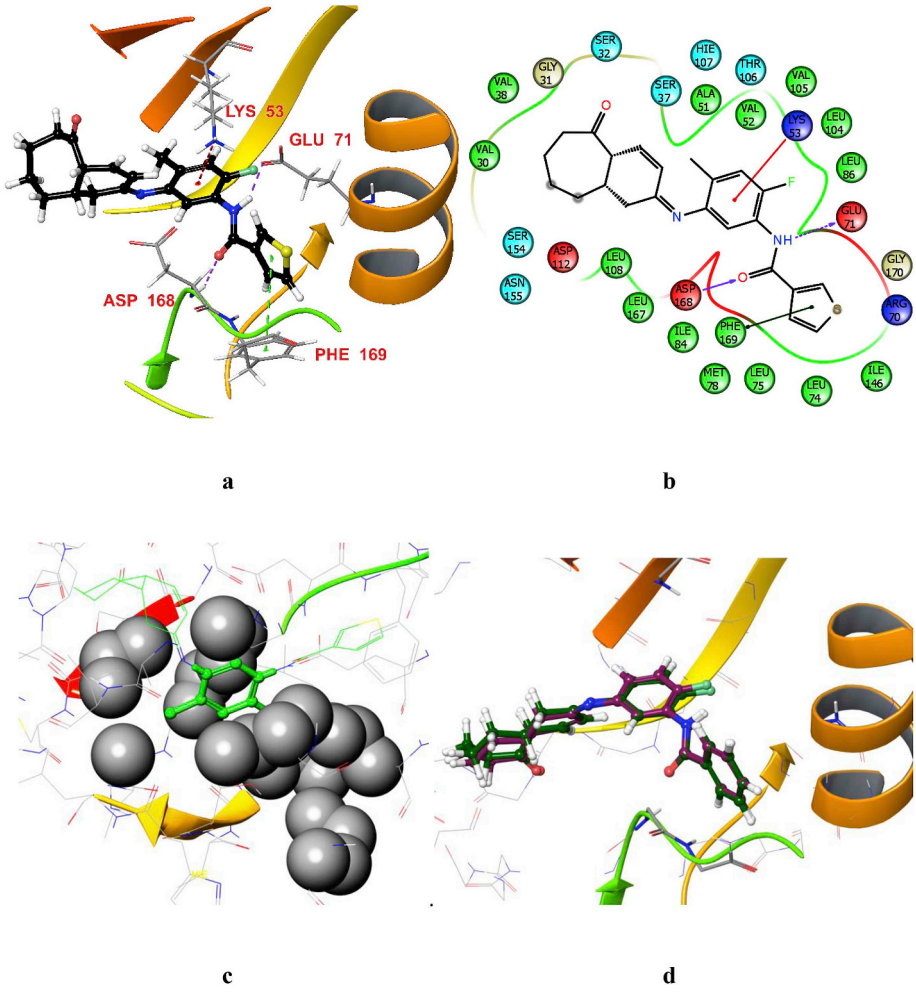

Fig. 6. (a) Binding mode of compound **48** in the catalytic pocket of **3UVP (b)** 2D-ligand interaction diagram of **48** in the catalytic pocket of **3UVP (c)** Hydrophobic interactions of **48** in the catalytic pocket of **3UVP (d)** Overlay of docked pose (magenta) of Benzamide Substituted Benzosuberone with its crystal structure conformation (green). (For interpretation of the references to colour in this figure legend, the reader is referred to the Web version of this article.)

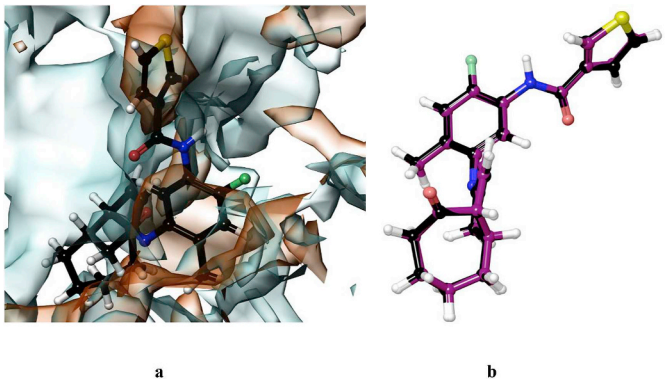

Fig. 7. (a) Map of hydrophobic and hydrophilic fields for inhibitor **48** into the catalytic pocket of protein MAP kinase **(3UVP).(b)**Superimposition of conformations of inhibitor **48**: best docking pose and pose of the DDHRR.8 model (RMSD: 0.090 Å).

to be 120 ($Å^2$). The molecular surface area (MSA) having a 1.4 probe radius was calculated. The polar surface area (PSA), i.e. solvent accessible by solvent molecule contributed by O and N atoms only was found to be 95 ($Å^2$) and the rGyr of compound **48** in the binding pocket of MAP kinase fluctuated between 5.05 and 5.15 Å. Properties like MSA and rGyr remained consistent up to 10 ns and indicated the steady behaviour of the ligand.

4. Discussion

Cancer is a major public health problem worldwide and is one of the leading causes of death globally. In the United States, it has been projected that, in 2019, 1,762,450 new cancer cases and 606,880 cancer deaths will occur [42]. MAP kinases regulate an extensive variety of cellular behaviours in response to extracellular stimuli. p38 MAP kinases are associated with an array of complex biological processes, like cell differentiation, cell proliferation, cell migration, cell death and invasion. p38 MAPK dysregulation may lead to reduced survival and advanced disease in cancer patients [43].

The present study performed 3D-QSAR studies and pharmacophore generation for a series of dibenzepinones, dibenzoxepines and benzosuberones based on p38α MAP kinase inhibitors. Our research group has reported such similar QSAR studies for compounds targeting EGFR and tubulin [10,11]. Apart from our research group, several other researchers across the globe are involved in such studies. The Patel group developed a structure-activity correlation model using 3D-QSAR, pharmacophore and docking studies for combretastatin A-4 based thiophene derivatives [44]. Almerico et al. performed 3D-QSAR,

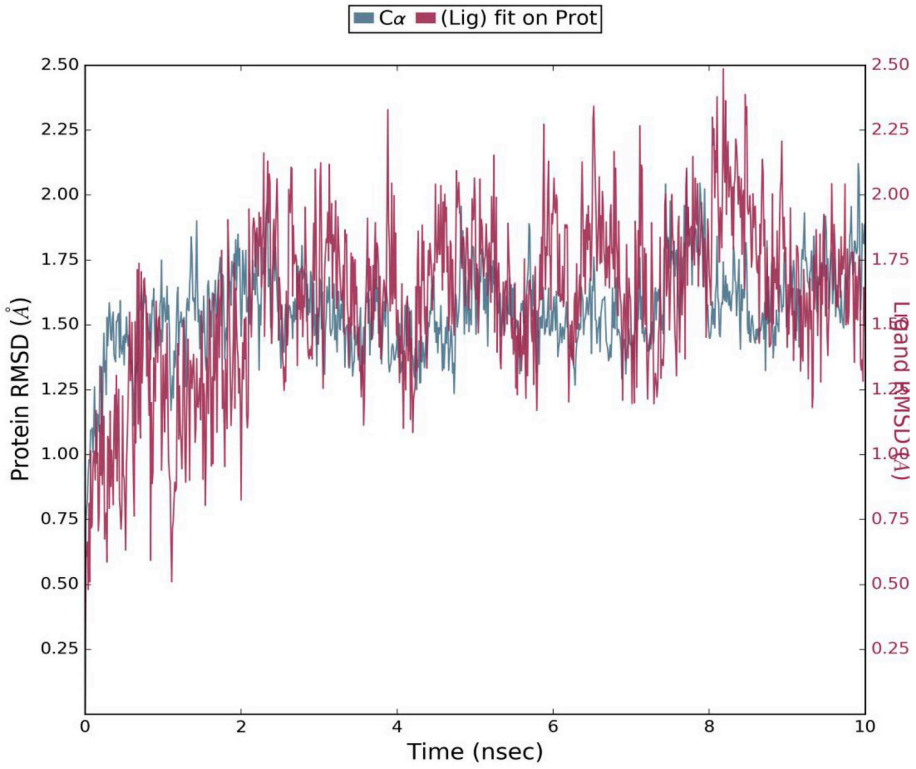

Fig. 8. RMSD plot of backbone of p38 MAPK- compound **48** complex.

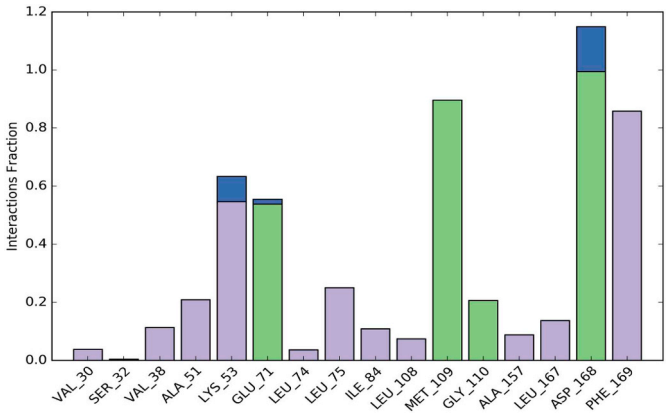

Fig. 9. Hydrogen and Hydrophobic Interactions of compound **48** from simulation trajectory.

pharmacophore modelling and *in silico* screening for novel BCl-xl inhibitors [45]. Palakurti and Vadrevu conducted pharmacophore-based 3D-QSAR modelling, virtual screening and docking for identification of potential inhibitors of β-secretase [46]. Several other studies relating 3D-QSAR, pharmacophore generation and molecular docking are available in the literature [47–49].

Several research groups have also performed QSAR studies on p38α MAP kinase inhibitors [50]. Pourbasheer et al. predicted QSAR for a series of novel pyrazole derivatives inhibiting p38α MAP kinase [51]. The Chang group also performed 3D-QSAR, comparative molecular field analysis (CoMFA) and comparative molecular similarity index analysis (CoMSIA) for 4-benzoyl-5-aminopyrazole derivatives. All these studies were carried out to identify the structural requirements for the development of new p38α MAP kinase inhibitors [52]. Various other research groups have also reported similar 3D-QSAR studies for a number of structurally diverse p38α MAP kinase inhibitors [53–55].

It is worth mentioning here that, before our study, no research group has reported targeting p38α MAP kinase with dibenzepinone, dibenzoxepine and benzosuberone groups. The pharmacophore model generated by our group exhibited good statistical correlation values like R^2 and Q^2. The reason for this good statistical correlation was the broad range of activity of the compounds that were chosen for generating the pharmacophore model. In order to assign the compounds to the training test set, compounds were selected from the complete range of activity. This was done to have compounds with significant diversity in activity. However, while developing the model, both activity and structural diversity were taken into consideration. Structural diversity is depicted by the different classes of compounds (dibenzepinone, dibenzoxepine and benzosuberone) included for model generation.

Furthermore, the developed model passed all the validation tests that are considered mandatory for a model to be reliable. These tests include external validation, Tropsha's test for predictive ability, the Y-randomisation test and domain of applicability (APD). The decoy test and ROC analysis were also performed to check the restrictivity of the model with inactive compounds by enrichment studies. Hence, our model can be considered a useful tool for the prediction of novel compounds.

5. Conclusion

In the present study, the structural basis and inhibitory mechanism was evaluated for certain MAP kinase inhibitors using a combined computational approach. In order to obtain insight into the structure-activity relationship, 3D-QSAR modelling was carried out. DDHRR.8, a model generated using atom-based 3D-QSAR, provided a good correlation and predictive power, thereby leading to a satisfactory agreement between experimental and theoretical results. Validation of the

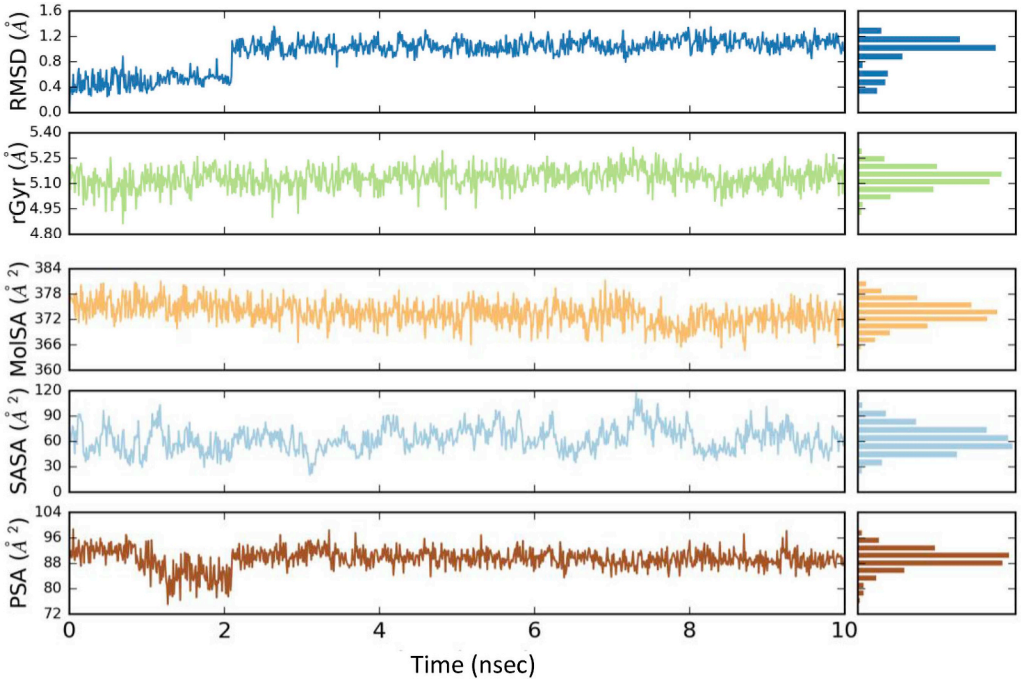

Fig. 10. Ligand Properties in terms of PSA, SASA and rGYR proving stablity of compound **48** into binding pocket.

generated model was also done using a certain number of tests, leading to further strengthening of the predictive power of the model. Additionally, molecular docking and dynamic studies were performed to identify the plausible binding poses of these inhibitors in the MAP kinase protein. These findings may be of immense importance in anticancer drug development, particularly for dibenzepinone-, dibenzoxepine- and benzosuberone-based p38α MAP kinase inhibitors.

Acknowledgements

The authors would like to thank Bioinformatics Facility, Jamia Hamdard, New Delhi, India.

Appendix A. Supplementary data

Supplementary data to this article can be found online at https://doi.org/10.1016/j.compbiomed.2019.05.023.

Funding

This research did not receive any specific grant from funding agencies in the public, commercial, or not-for-profit sectors.

Declaration of interest

The Authors declare no conflict of interest.

Conflicts of interest

Authors declare no conflict of interest.

References

[1] A.A. Patravale, A.H. Gore, G.B. Kolekar, M.B. Deshmukh, P.B. Choudhari, M.S. Bhatia, S. Prabhu, M.D. Jamdhade, M.S. Patole, P.V. Anbhule, Synthesis, biological evaluation and molecular docking studies of some novel indenospiro derivatives as anticancer agents, J. Taiwan Inst. Chem. Eng. 68 (2016) 105–118.

[2] P.C. Nagajyothi, P. Muthuraman, T.V.M. Sreekanth, D.H. Kim, J. Shim, Green synthesis: *in-vitro* anticancer activity of copper oxide nanoparticles against human cervical carcinoma cells, Arab. J. Chem. 10 (2017) 215–225.

[3] P. Yadav, K. Lal, A. Kumar, S. Bhushan, S.K. Guru, S. Jaglan, Green synthesis and anticancer potential of chalcone linked-1,2,3-triazoles, Eur. J. Med. Chem. 126 (2017) 944–953.

[4] J.S. Sebolt-Leopold, Development of anticancer drugs targeting the MAP kinase pathway, Oncogene 19 (2000) 6594–6599.

[5] K. Burkhard, P. Shapiro, Use of inhibitors in the study of MAP kinases, Methods Mol. Biol. 661 (2010) 107–122.

[6] S. Horjales, D. Schmidt-Arras, R.R. Limardo, O. Leclercq, G. Obal, E. Prina, A.G. Turjanski, G.F. Spath, A. Buschiazzo, The crystal structure of the MAP kinase LmaMPK10 from *Leishmania Major* reveals parasite-Specific features and regulatory mechanisms, Structure 20 (2012) 1649–1660.

[7] C.I. Chang, B. Xu, R. Akella, H.M. Cobb, E.J. Goldsmith, Crystal structures of MAP kinase p38 complexed to the docking sites on its nuclear substrate MEF2A and activator MKK3b, Mol. Cell 9 (2002) 1241–1249.

[8] J.C. Dearden, The history and development of quantitative structure-activity relationships (QSARs), Int. J. Quant. Struct.-Prop. Relatsh. 1 (2016) 1–44.

[9] K. Roy, S. Kar, R.N. Das, Applications in Pharmaceutical Sciences and Risk Assessment, first ed., Academic Press, 2015.

[10] M.F. Khan, G. Verma, W. Akhtar, M. Shaquiquzzaman, M. Akhter, M.A. Rizvi, M.M. Alam, Pharmacophore modeling, 3D-QSAR,docking study and ADME prediction of acyl 1,3,4-thiadiazole amides and sulfonamides as antitubulin agents, Arab. J. Chem. (2016), https://doi.org/10.1016/j.arabjc.2016.11.004.

[11] G. Verma, M.F. Khan, W. Akhar, M.M. Alam, M. Akhter, O. Alam, S.M. Hasan, M. Shaquiquzzaman, Pharmacophore modeling, 3D-QSAR, docking and ADME prediction of quinazoline based EGFR inhibitors, Arab. J. Chem. (2016), https://doi.org/10.1016/j.arabjc.2016.09.019.

[12] N. Basant, C. Durante, M. Cocchi, M.\.C. Menziani, Modeling the binding affinity of p38α MAP kinase inhibitors by partial least squares regression, Chem. Biol. Drug Des. 80 (2012) 455–470.

[13] R.S. Nayan, S.K. Bommisetty, K. Singh, S.K. Bairy, S. Nunna, A. Pramod, R. Muttineni, Structural analysis of carboline derivatives as inhibitors of MAPKAP K2 using 3D QSAR and docking studies, J. Chem. Inf. Model. 49 (2009) 53–67.

[14] C. Huang, Y. Li, H. Ren, J. Wang, L. Shao, S. Zhang, G. Li, L. Yang, Insight into the structural determinants of imidazole scaffold-based derivatives as p38 MAP kinase inhibitors by computational explorations, Curr. Med. Chem. 19 (2012) 4024–4037.

[15] K.E. Martz, A. Dorn, B. Baur, V. Schattel, M.I. Goettert, S.C. Mayer-Wrangowski, D. Rauh, S.A. Laufer, Targeting the hinge glycine flip and the activation loop: novel approach to potent p38α inhibitors, J. Med. Chem. 55 (2012) 7862–7874.

[16] M. Goettert, R. Graeser, S.A. Laufer, Optimization of a nonradioactive immunosorbent assay for p38alpha mitogen-activated protein kinase activity, Anal. Biochem. 406 (2010) 233–234.

[17] D. Shivakumar, J. Williams, Y. Wu, W. Damm, J. Shelley, W. Sherman, Prediction of absolute solvation free energies using molecular dynamics free energy perturbation and the OPLS force field, J. Chem. Theory Comput. 6 (2010) 1509–1519.

[18] S.L. Dixon, A.M. Smondyrev, E.H. Knoll, S.N. Rao, D.E. Shaw, R.A. Friesner, PHASE: a new engine for pharmacophore perception, 3D QSAR model development, and 3D database screening: 1. Methodology and preliminary results, J. Comput. Aided Mol. Des. 20 (2006) 647–671.

[19] N.S. Tripuraneni, M.A. Azam, Pharmacophore modeling, 3D-QSAR and docking study of 2-phenylpyrimidine analogues as selective PDE4B inhibitors, J. Theor. Biol. 394 (2016) 117–126.
[20] G.M. Sastry, S.L. Dixon, W. Sherman, Rapid shape-based ligand alignment and virtual screening method based on atom/feature-pair similarities and volume overlap scoring, J. Chem. Inf. Model. 51 (2011) 2455–2466.
[21] M.D. Miller, R.P. Sheridan, S.K. Kearsley, S.Q., A program for rapidly producing pharmacophorically relevant molecular superpositions, J. Med. Chem. 42 (1999) 1505–1514.
[22] G. Melagraki, A. Afantitis, Enalos KNIME nodes: exploring corrosion inhibition of steel in acidic medium, Chemometr. Intell. Lab. Syst. 123 (2013) 9–14.
[23] E. Vrontaki, G. Melagraki, T. Mavromoustakos, A. Afantitis, Searching for anthranilic acid-based thumb pocket 2 HCV NS5B polymerase inhibitors through a combination of molecular docking, 3D-QSAR and virtual screening, J. Enzym. Inhib. Med. Chem. 31 (2016) 38–52.
[24] S. Zhang, A. Golbraikh, S. Oloff, H. Kohn, A. Tropsha, A novel automated lazy learning QSAR (ALL-QSAR) approach: method development, applications, and virtual screening of chemical databases using validated ALL-QSAR models, J. Chem. Inf. Model. 46 (2006) 1984–1995.
[25] J. Kirchmair, P. Markt, S. Distinto, G. Wolber, T. Langer, Evaluation of the performance of 3D virtual screening protocols: RMSD comparisons, enrichment assessments, and decoy selection-What can we learn from earlier mistakes? J. Comput. Aided Mol. Des. 22 (2008) 213–228.
[26] R.P. Sheridan, S.B. Singh, E.M. Fluder, S.K. Kearsley, Protocols for bridging the peptide to nonpeptide gap in topological similarity searches, J. Chem. Inf. Comput. Sci. 41 (2001) 1395–1406.
[27] J.T. Patrisha, M. Battu, D. Sriram, P. Yogeeswari, 3D-QSAR studies combined with virtual screening to identify novel inhibitors of N-acetyl glucosamine 1-phosphate uridyltransferase from Mycobacterium tuberculosis, Int. J. Drug. Des. Discov. 4 (2013) 1134–1148.
[28] A. Tropsha, P. Gramatica, V.K. Gombar, The importance of being earnest: validation is the absolute essential for successful application and interpretation of QSPR models, QSAR Comb. Sci. 22 (2003) 69–77.
[29] K. Roy, R.N. Das, P. Ambure, R.B. Aher, Be aware of error measures. Further studies on validation of predictive QSAR models, Chemometr. Intell. Lab. Syst. 152 (2016) 18–33.
[30] K. Roy, P. Ambure, R.B. Aher, How important is to detect systematic error in predictions and understand statistical applicability domain of QSAR models? Chemometr. Intell. Lab. Syst. 162 (2017) 44–54.
[31] M. Shen, C. Beguin, A. Golbraikh, J. Stables, H. Kohn, A. Tropsha, Application of predictive QSAR models to database Mining: identification and experimental validation of novel anticonvulsant compounds, J. Med. Chem. 47 (2004) 2356–2364.
[32] A. Afantitis, G. Melagraki, H. Sarimveis, P.A. Koutentis, J. Markopoulos, O. Igglessi-Markopoulou, Development and evaluation of a QSPR model for the prediction of diamagnetic susceptibility, QSAR Comb. Sci. 27 (2008) 432–436.
[33] G.M. Sastry, M. Adzhigirey, T. Day, R. Annabhimoju, W. Sherman, Protein and ligand preparation: parameters, protocols and influence on virtual screening enrichments, J. Comput. Aided Mol. Des. 27 (2013) 221–234.
[34] R.A. Friesner, R.B. Murphy, M.P. Repasky, L.L. Frye, J.R. Greenwood, T.A. Halgren, P.C. Sanschagrin, D.T. Mainz, Extra precision glide: docking and scoring incorporating a model of hydrophobic enclosure for protein-ligand complexes, J. Comput. Aided Mol. Des. 49 (2006) 6177–6196.
[35] N.S. Tripuraneni, M.A. Azam, A combination of pharmacophore modeling, atom-based 3D-QSAR, molecular docking and molecular dynamics simulation studies on PDE4 enzyme inhibitors, J. Biomol. Struct. Dyn. 34 (2016) 2481–2492.
[36] M.F. Khan, M.M. Alam, G. Verma, W. Akhtar, M.A. Rizvi, A. Ali, M. Akhter, M. Shaquiquzzaman, Molecular interactions of dioxins and DLCs with the ketosteroid receptors: an in silico risk assessment approach, Toxicol. Mech. Methods 27 (2017) 151–163.
[37] M.P. Jacobson, D.L. Pincus, C.S. Rapp, T.J.F. Day, B. Honig, D.E. Shaw, R.A. Friesner, A hierarchical approach to all-atom protein loop prediction, Proteins 55 (2004) 51–367.
[38] J. Li, R. Abel, K. Zhu, Y. Cao, S. Zhao, R.A. Friesner, The VSGB2.0 model: a next generation energy model for high resolution protein structure modeling, Proteins 79 (2011) 2794–2812.
[39] B. Baur, K. Storch, K.E. Martz, M.I. Goettert, A. Richters, D. Rauh, S.A. Laufer, Metabolically stable dibenzo[b,e]oxepin-11(6H)-ones as highly selective p38 MAP kinase inhibitors: optimizing anti-cytokine activity in human whole blood, J. Med. Chem. 56 (2013) 8561–8578.
[40] A. Golbraikh, A. Tropsha, Beware of q2!, J. Mol. Graph. Model. 20 (2002) 269–276.
[41] A. Golbraikh, A. Tropsha, Predictive QSAR modeling based on diversity sampling of experimental datasets for the training and test set selection, J. Comput. Aided Mol. Des. 5 (2002) 231–243.
[42] R.L. Siegel, K.D. Miller, A. Jemal, Cancer statistics, 2019, Ca - Cancer J. Clin. 69 (2019) 7–34.
[43] H.K. Koul, M. Pal, S. Koul, Role of p38 MAP kinase signal transduction in solid tumors, Genes Cancer 4 (2013) 342–359.
[44] V.K. Patel, A. Singh, D.K. Jain, P. Patel, R. Veerasamy, P.C. Sharma, H. Rajak, Combretastatin A-4 based thiophene derivatives as antitumor agent: development of structure activity correlation model using 3D-QSAR, pharmacophore and docking studies, Future J. Pharm. Sci. 3 (2017) 71–78.
[45] A.M. Almerico, M. Tutone, A. Lauria, 3D-QSAR pharmacophore modeling and in silico screening of new Bcl-xl inhibitors, Eur. J. Med. Chem. 45 (2010) 4774–4782.
[46] R. Palakurti, R. Vadrevu, Pharmacophore based 3D-QSAR modeling, virtual screening and docking for identification of potential inhibitors of β-secretase, Comput. Biol. Chem. 68 (2017) 107–117.
[47] K.S. Bhadoriya, M.C. Sharma, S.V. Jain, Pharmacophore modeling and atom-based 3D-QSAR studies on amino derivatives of indole as potent isoprenylcysteine carboxyl methyltransferase (Icmt) inhibitors, J. Mol. Struct. 1081 (2015) 466–476.
[48] X. Zhang, H. Zhang, 3D-QSAR studies on 1,2,4-triazolyl 5-azaspiro [2.4]-heptanes as D3R antagonists, Chem. Phys. Lett. 704 (2018) 11–20.
[49] J. Tong, Y. Wu, M. Bai, P. Zhan, 3D-QSAR and Molecular Docking Studies on HIV Protease Inhibitors vol. 1129, (2017), pp. 17–22.
[50] R.P. Gangwal, A. Bhadauriya, M.V. Damre, G.V. Dhoke, A.T. Sangamwar, p38 mitogen-activated protein kinase inhibitors: a review on pharmacophore mapping and QSAR studies, Curr. Top. Med. Chem. 13 (2013) 1015–1035.
[51] E. Pourbasheer, S. Ahmadpour, R. Zare-Dorabei, M. Nekoei, Quantitative structure activity relationship study of p38a MAP kinase inhibitors, Arab. J. Chem. 10 (2017) 33–40.
[52] H.-W. Chang, F.-S. Chung, C.-N. Yang, Molecular modeling of p38α mitogen-activated protein kinase inhibitors through 3d-QSAR and molecular dynamics simulations, J. Chem. Inf. Model. 53 (2013) 1775–1786.
[53] M. Shahlaei, E. Doosti, Virtual screening based on pharmacophore model followed by docking simulation studies in search of potential inhibitors for p38 map kinase, Biomed. Pharmacother. 80 (2016) 352–372.
[54] E.G. Hadajia, M. Bourassa, A. Ouammoua, M. Bouachrine, 3D-QSAR models to predict anti-cancer activity on a series ofprotein P38 MAP kinase inhibitors, J. Taibah U. Sci. 11 (2017) 392–407.
[55] Z. Ul-Haq, W. Khan, S.R. Zia, S. Iqbal, Structure-based 3D-QSAR models and dynamics analysis of novel N-benzyl pyridinone as p38α MAP kinase inhibitors for anticytokine activity, J. Mol. Graph. Model. 36 (2012) 48–61.